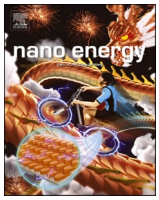
Nano Energy 128 (2024) 109821



Contents lists available at ScienceDirect

Nano Energy

journal homepage: www.elsevier.com/locate/nanoen





Biomimetic fiber of PVDF@Ag enabling the multimodal sensing for biomechanics and biomolecules integrated by textile carrier

Dongzhen Chen [a], Yang Li [a], Jianzhao Gao [a], Meng Zhang [c], Junhao Liang [a], Tao Fu [d], Xiaoming Wu [d], Xinhai He [a], Liangjun Xia [b,*], Weilin Xu [b,*]

[a] School of Materials Science & Engineering, Key Laboratory of Functional Textile Material and Product of the Ministry of Education, Xi'an Key Laboratory of Textile Composites, Xi'an Polytechnic University, Xi'an 710048, China
[b] State Key Laboratory of New Textile Materials and Advanced Processing Technologies, Wuhan Textile University, Wuhan 430200, China
[c] Department of Neurology, The First Affiliated Hospital of Xi'an Jiaotong University, Xi'an, Shaanxi 710061, China
[d] Key Laboratory of Biomedical Information Engineering of Ministry of Education, School of Life Science and Technology, Xi'an Jiaotong University, Xi'an 710049, China

ARTICLE INFO

Keywords:
Wearable sensing
Biomechanics and biomolecule
PVDF@Ag fiber
Textile carrier
Healthcare management

ABSTRACT

Intelligent wearables with integrated biomechanics and biomolecule multimodal sensing systems are crucial for personalized healthcare. However, the modes of action of biomechanics and biomolecule sensing work in different ways. Hence, a method for manufacturing biomimetic fibers made of polyvinylidene fluoride (PVDF) @silver (Ag) is initially devised, and a textile carrier serves as a link for multimodal sensing of biomechanics and biomolecules. PVDF nanofiber membranes are created using a one-step electrospinning process. Next, by lowering the silver ion's reduction potential, compact and homogenous Ag nanoparticles (NPs) are formed *in-situ* on the high-curvature PVDF fibers. Consequently, a PVDF@Ag fiber membrane with a piezoelectric response and a localized surface plasmon resonance (LSPR) effect is created, making it suitable for wearable sensors that can detect secreta molecules as well as muscle movements. PVDF@Ag fiber is twisted, taking inspiration from the spiral structure of butterfly antennae. Compared to untwisted, twisted PVDF@Ag fiber, this produces a surface-enhanced Raman scattering (SERS) output signal that is more stable and can resist for signal attenuation caused by tensile deformation during wearable sensing. The "fingerprint" spectra of SERS enable noninvasive extraction and detection of secretion signals at sweat and respiration. Additionally, a plausible correlation between the range of secretions produced and health-related data is examined. Additionally, the integrated PVDF@Ag by polyester fabric exhibits superior air permeability, moisture absorption, and antimicrobial properties. And, this multimodal sensing mechanism has an algorithm implanted with deep learning support. All things considered, the PVDF@Ag fiber functions as a bridge between biomolecules and biomechanics, which is essential for applications involving wearable healthcare management.

1. Introduction

There is a connection between wearable biomechanics and biomolecules sensing on the skin and future tailored health care [1,2]. A seamless evaluation of life health benefits greatly from merging biomechanics detection and biomolecule recognition in addition to breaking through the barrier in a typical stiff sensor [3–5]. Using multiplex sensing mechanisms to monitor biomolecules and biomechanics simultaneously, such heart rate, [1], muscle activities [6–11] and perspiration [12] is a persuasive approach. A number of piezoresistive or piezoelectric wearable sensors have found successful applications during the last ten years, such as those for vibrating voice cords, breathing movements, physical activity, pulse vibration, and more [13]. However, real-time molecular health monitoring, which is essential for accurate individual diagnosis and customization of a physical sign, is still lagging due to the lack of wearable analysis technology of molecules at the epidermis. Currently, popular wearable bio/chemical sensing technique is electrochemical analysis, where specific current or potential measurement is employed to analyze electrolytes (K^+ and Na^+) [14–18] and metabolites (lactate and glucose) concentrations in sweat [19–21]. However, these sensors are limited to detecting a single target molecule at a time and frequently fail to offer

* Corresponding authors.
E-mail addresses: liangjun_xia@wtu.edu.cn (L. Xia), weilin_xu@wtu.edu.cn (W. Xu).

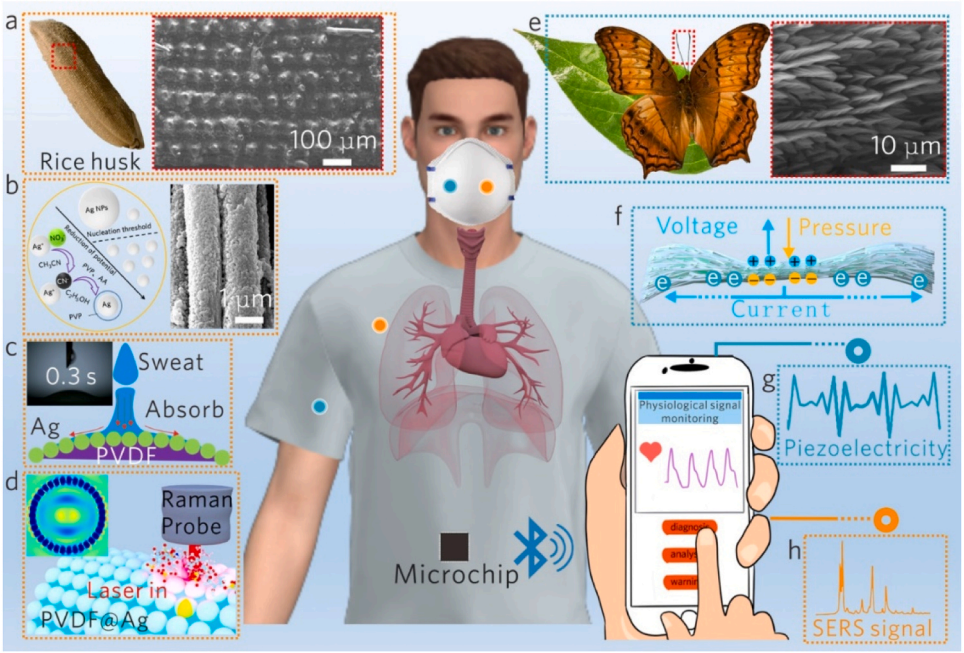
https://doi.org/10.1016/j.nanoen.2024.109821
Received 25 March 2024; Received in revised form 9 May 2024; Accepted 31 May 2024
Available online 31 May 2024
2211-2855/© 2024 Elsevier Ltd. All rights are reserved, including those for text and data mining, AI training, and similar technologies.

essential biomechanics on the human body. To evaluate health status, however, combined sensing for biomechanics and biomolecules is typically necessary in order to get all pixels of dynamic health information [12]. Thus, the next advancement in wearable health monitoring might be multimodal detection for muscular strain and epidermal secretion combined via clothes carrier. Flexible plasmonic nanofiber membranes have attracted a lot of attention because of their excellent clothing integration qualities, electroconductivity, and photo-response at the nanoscale scale [22,23].

Because of high porosity, excellent mechanical property and large surface area to volume ratio, electrospinning is a valuable method for fabricating diverse functional nanofibers as photoelectronic devices [24], bionics [25] and optical sensors [26]. For instance, electrospun Au/thermoplastic polyurethane nanofibers were employed to detect the pH of sweat by surface-enhanced Raman scattering (SERS) spectroscopy [27], which not only preserve the fast, noninvasive, and label-free detection but also address the drawback of the weaker Raman signal strength [22,23]. The polyvinylidene fluoride (PVDF) fiber is an excellent piezoelectric material [28–30]. Fan *et al.* develop a sweat permeable PVDF piezoelectric nanoyarns by three-dimensional textile technology, which provides a practical strategy for developing comfortable wearable electronic devices [28]. However, one practical strategy for achieving multimodal sensing could be to plasmonically functionalize PVDF fiber. For example, a sort of electrospun PVDF@Au nanofiber was developed for bacteria detection using SERS spectrum in our previous study [23]. And, in order to achieve sufficient piezoelectricity, the β-phase of PVDF must be preserved during the plasmonic functionalization process. It is therefore crucial to preserve the piezoelectricity during the plasmonic functionalization process, since this could result in both a sensitive piezoelectric signal and a stable SERS signal.

It is foreseeable that wearable health detection will eventually grow along the path of clothing integration [5]. For example, Tao *et al.* present a braided electronic cord strategy based on the core-spun pressure-sensing yarn technique [31], through artificial intelligence technology acting as a cognitive engine and multifunctional textile acting as sensing units, which would pave the path for wearable medicine and healthcare. Nevertheless, the use of plasmonic devices for wearable sensing is still relatively new; the primary challenge is preserving structural stability in the face of repeated physical activity and muscle contractions. For example, the nano-gap created at the plasmonic sensor array often retains localized surface plasmon resonance (LSPR) activity and is highly sensitive to changes in the distance and structure of the nanometer scale. However, muscular movements will undermine the LSPR sensing ‘‘hot spots’’ structure, which will impact the wearable SERS detection outcome. In order to mitigate the effects of physical activity-induced deformation, Wang, Liu, *et al.* created a tiny guard ring to shield the Au superlattice’s ‘‘hot spots’’ structure from physical activity and maintain the stability of the SERS signal intensity [32]. Furthermore, compared to single-layer nanostructures, multilayered plasmonic nanostructures exhibit superior SERS signal homogeneity and stability according to our earlier research [33,34]. One possible design to withstand the effect of deformation during wearable SERS sensing is multilayered ‘‘hot spots’’. Furthermore, the anti-interference sensing methods are essential, particularly when it comes to taking advantage of wearable technology’s integrated bio/chemical and biomechanical sensors.

As a result, an intelligent pretreatment plan for PVDF@Ag biomimetic fiber was initially created. (Scheme 1). First, a one-step electrospinning procedure was used to create the PVDF nanofiber membrane. Second, by lowering the reduction potential of Ag^{+} ion, the compact and homogenous sliver nanoparticles (AgNPs) are formed *in-situ* on the high-curvature fibers of PVDF. Multiple contact surfaces, such as those made of rice husk (Scheme 1a and b), have a super hygroscopic capacity that makes them ideal for collecting sweat, absorbing moisture, and detecting SERS (Scheme 1c and d). Twisted fiber of PVDF@Ag is designed with inspiration from the spiral structure of butterfly antennae (Scheme 1e). This results in a SERS output signal that is more stable than untwisted, which could resist the signal decay caused by wearable tensile deformation. Consequently, a PVDF@Ag fiber with various piezoelectric response and LSPR effect capabilities was created, making it suitable for wearable muscle movement and secreta molecule monitoring (Scheme 1f, g, h). Thirdly, complex biomechanics and biomolecule signals are intended to be recognized by a machine learning system



Scheme 1. PVDF@Ag biomimetic fiber enables wearable biomechanics and biomolecules sensing. (a) Microscopic surface of rice husk. (b) The PVDF@Ag biomimetic preparation preferred the rice husk surface. (c) The highly hygroscopic PVDF@Ag fiber was attracted to rice husks. (d) Detection of molecules in sweat by localized surface plasmon resonance effect. (e) Microscopic surface of the antennae of the butterfly. Wearable health monitoring using biomechanics (f and g) and biomolecules (h).

that integrates the PVDF@Ag fibers. Additionally, a precise survey comparing the physiological data of the human body with the output spectrum of secretions is also looked into. Overall, the PVDF@Ag fiber fills the detection gap between the biomolecule and biomechanics. Using an integrated sensing mechanism like this one allows wearable sensing to prioritize human health assessment.

2. Results and discussion

2.1. PVDF@Ag fiber preparation and characterization

Four procedures were used to prepare the PVDF@Ag flexible membrane (Fig. 1a–d). A straightforward one-step electrospinning technique was used to create the PVDF nanofiber membrane that doped the hydroxylamine hydrochloride (HHE) (Fig. 1a). PVDF, being a polycrystalline polymer, exhibits three distinct chain conformations: (i) the β-phase of the planar zigzag all-trans (TTTT) conformation, (ii) the α- and δ-phases of the alternating trans-gauche (TGTG′) conformations, and (iii) the γ- and ε-phases of the T3GT3G′ conformation. [30]. Because of the electrostatic repulsion and high reduction rate of Ag^+, direct growth of AgNPs on the PVDF fiber is challenge. Hence, an Au seed-mediated synthesis is employed for fabrication of nanofiber of PVDF@Ag. Firstly, ethanol is employed to induce the phase transformation from α-phase to the β-phase, the loading of Au seeds was achieved by mixing PVDF with solution of $HAuCl_4$, and $HAuCl_4$ was reduced by $NaBH_4$ (Fig. S1). The above method of successive ionic layer adsorption reaction was also studied (Fig. 1c and Fig. 1e_1–e_4). By using this method, Au seeds can sprout on the PVDF fiber surface; however, at cycles 2, 4, 6, and 8, the Au seeds (approximately 20 nm) are sparsely grown on the PVDF surface (Fig. 1e_1–e_4). Au seeds displayed partial aggregation on PVDF fiber surface as growth cycles increased (Fig. 1e_4). Through the above experimental research, successive adsorbent growth is impossible to produce compact and uniform Au and Ag nanoparticles on the high curvature fiber of PVDF, which limits the fabrication of plasmonic nano-sensors of PVDF fibers. Finally, the nanofiber membrane of PVDF@Ag prepared by seeds-mediated and potential-lowed reduction are shown in Fig. 1f_1–f_4, and photographs of fibrous membrane of PVDF@Ag are shown in Fig. S2. Nanofiber of PVDF@Ag is made up of five main elements of C, F, O, Ag and Au (Fig. 1g_1–g_5 and Fig. S3).

Controlling the pace of reduction reaction is the key to creating PVDF@Ag nanofiber with a homogeneous and dense distribution of AgNPs. Due to the high reduction potential of Ag^+ ions, self-nucleation occurred when ascorbic acid reducer was combined with Ag^+ ions,

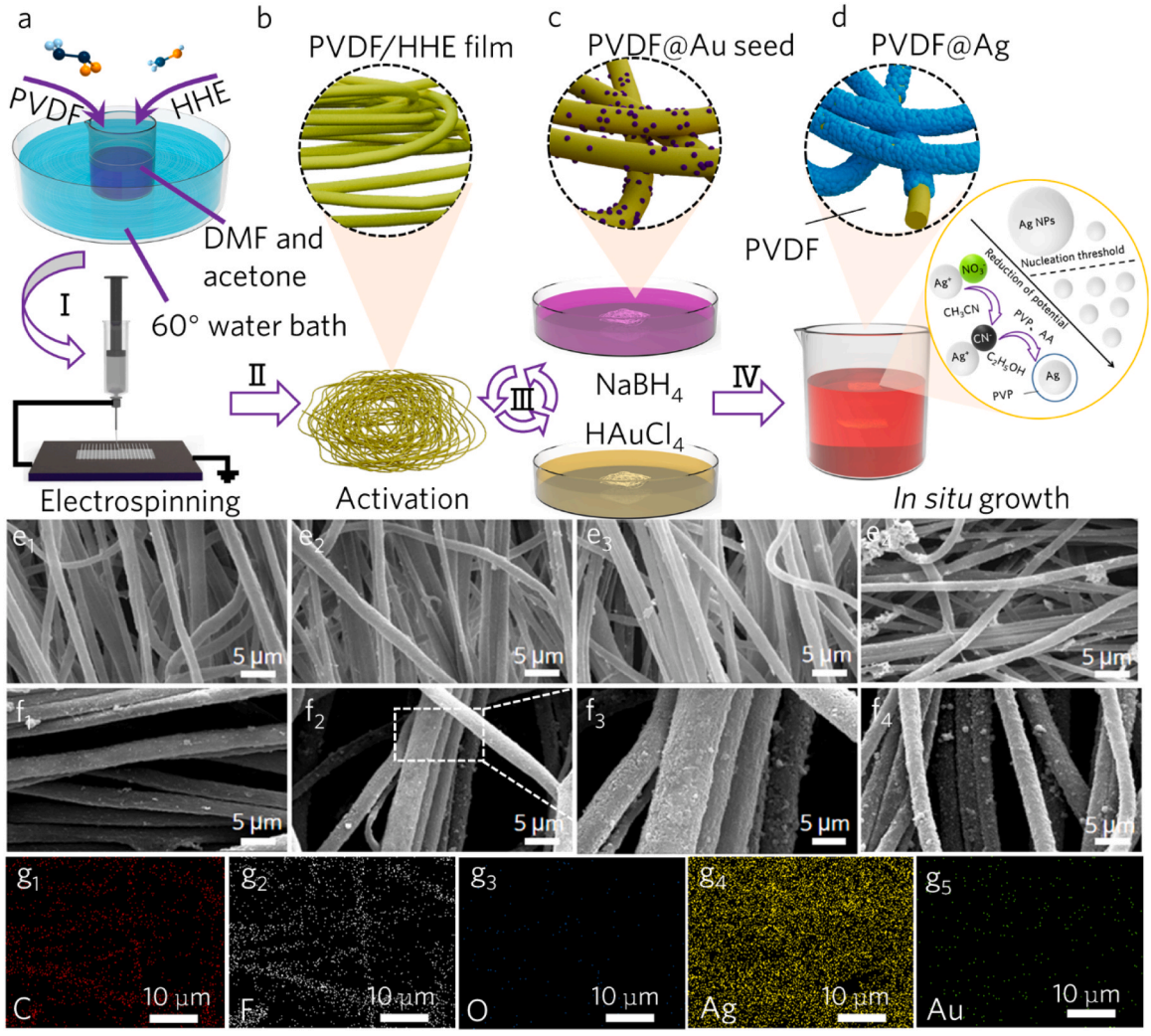


Fig. 1. Illustration of the fabrication process of the fiber membrane of polyvinylidene fluoride (PVDF)@Ag. (a) and (b) electrospinning preparation of PVDF nanofiber membrane by doping the hydroxylamine hydrochloride (HHE); (c) PVDF@Au seeds was prepared by repetitive ionic layer adsorption reaction, where $HAuCl_4$ was reduced by $NaBH_4$; (d) PVDF@Au seeds-mediated synthesis is used for fabrication of PVDF@Ag nanofiber; (e_1-e_4) SEM images of PVDF@Au seeds prepared by ionic layer adsorption reaction of 2, 4, 6 and 8 times; (f_1-f_4) SEM images of fiber membrane of PVDF@Ag through potential-lowed and seeds-mediated reduction; (g_1-g_5) EDS element mapping of PVDF@Ag membrane's C, F, O, Ag, and Au.

resulting in the deposition of a small amount of AgNPs on PVDF fiber. Based on our previous study [23,34], $AgNO_3$ was employed as the metal source, ascorbic acid as reductant, acetonitrile as coordinating ligand, ethanol as surface modifier and polyvinyl pyrrolidone (PVP) as the additional capping ligand. The nitrile group present in acetonitrile has the ability to bind with Ag^+ ions to decrease their reduction potential, hence preventing self-nucleation.

By inserting the PVDF@Au seeds into the growth fluid, the seeded growth of PVDF@Ag was started. The generated outcomes of a range of growth solutions in the absence of ethanol, acetonitrile, or PVP are displayed in Fig. 2a–c, respectively, to further demonstrate the crucial significance of recipe. However, the surface of PVDF fibers has significant blank patches and uneven AgNP aggregation (Fig. 2a–c). PVP is often a type of capping ligand that can disperse nanostructures and stabilize atomic monomers [23]. Additionally, we discovered that the nitrile group plays a key role in promoting the *in-situ* growth of AgNPs on the PVDF fiber surface and inhibiting the self-nucleation process. As seen by the UV–vis spectrum of the growth solution in Fig. S4, when PVP, Ag^+ ion, and ascorbic acid were combined without acetonitrile, there was a clear self-nucleation of AgNPs. This further establishes the critical role of acetonitrile. Ag atoms may germinate on the surface of PVDF nanofibers, acetonitrile coordination may decrease the Ag^+ ion's reduction potential, and Au seeds may encourage the reduction of Ag^+ ions. Ag nanoparticles with a homogeneous and dense distribution could be formed on PVDF's high curvature fiber using this seed-motivated reduction technique (Fig. 2d and Fig. S5).

Through the use of FTIR spectra and XRD patterns, the phase transition and adsorption mechanism between the PVDF and Au/Ag contact were examined. The FTIR spectra and XRD patterns of PVDF, PVDF@Au seeds, and PVDF@Ag nanofiber are displayed in Fig. 2e and f. The FTIR spectra (Fig. 2e) demonstrated the PVDF nanofibers' relative β-phase content. Compared to pure PVDF membrane (Fig. S6), doping the HHE could improve the content of β-phase and restrain the vast decrease of β-phase during the plasma functionalization of PVDF fiber. Based on Lambert Beer's law [35,36], the content of β-phase is 87.2 % (PVDF-HHE), 85 % (PVDF@Au seeds) and 76.4 % (PVDF@Ag nanofiber). The content of β-phase shows a small drop after plasmonic functionalization of fiber PVDF-HHE, in contrast to the undoped PVDF of HHE, but which is adequate for piezoelectric response sensing [23,29].

Although ethanol cannot dissolve PVDF, it can induce the molecular chains to phase convert on the surface at shallow depths. As the ethanol evaporation, the β-phase will gradually turn into amorphous or other phases. Additionally, bits of β-phase are held on the PVDF surface due to $AuCl_4^-$ coordination, which aids in the germination of Au seeds on the PVDF fiber surface. Meanwhile, the XRD pattern shows five diffraction peaks at 2θ of 38.3°, 44.6°, 64.7° and 77.5° correspond to the (111), (200), (220) and (311) lattice plane of face centered cubic (*fcc*) Ag

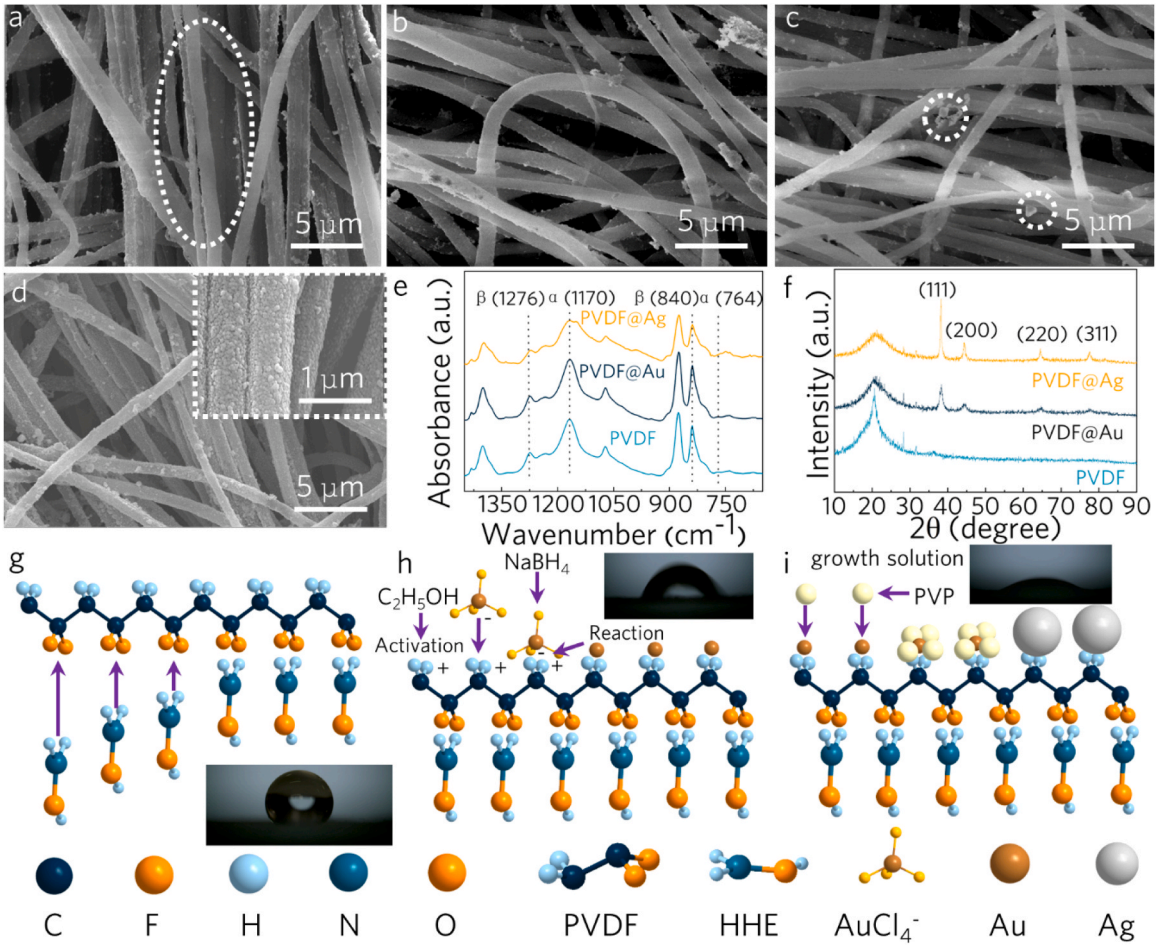


Fig. 2. Growth mechanism of Ag on the surface of PVDF fiber. $AgNO_3$, ascorbic acid, acetonitrile, PVP and PVDF@Au seeds made up the reactant in (a); $AgNO_3$, ascorbic acid, ethanol, polyvinyl pyrrolidone (PVP) and PVDF@Au seeds made up the reactant in (b); $AgNO_3$, ascorbic acid, acetonitrile, ethanol and PVDF@Au seeds made up the reactant in (c); $AgNO_3$, ascorbic acid, acetonitrile, PVP, ethanol and PVDF@Au seeds made up the reactant in (d); Where PVDF@Au seeds is introduced to initiate reduction of Ag^+ ion; (e) FT-IR spectra and (f) XRD pattern of membrane of PVDF, PVDF@Au seeds and PVDF@Ag nanofiber respectively; (g) Dipoles between $-NH_2$ groups of hydroxylamine hydrochloride and $-CF_2$ groups of PVDF chains; (h) Positive group on the PVDF surface is activated by ethanol; (i) Ag nanomonomers deposited on the PVDF surface with the Au seed as the site of nucleation.

(Fig. 2f) [37], and the diffraction peaks of 17.6°, 18.5° and 20.1° belong to (100), (020) and (110) crystal planes of α-phase respectively [30,38]. A strong peak located at 20.7° belong to (110) and (200) crystal planes of β-phase [30]. Furthermore, the phase transition of PVDF will be brought about by hydrogen bonding and the electrostatic interaction between C-F bonds and ethanol. Additionally, the electropositivity of PVDF nanofibers will be generated by the ordinal arrangement of CH_2 dipole (δ+) and it will adsorb $AuCl_4^-$ [23]. An all-trans β phase PVDF is formed when the high electric field and uniaxial stretch during electrospinning induce the molecular chain conformation of PVDF to rotate and arrange them parallel in the direction of the electric field (Fig. 2g). At the same time, in the electrospinning process, a large amount of -NH_2 groups contained in HHE can bond with negatively charged -CF_2 groups in PVDF to form NH_2-CF_2 dipoles. The positively charged -CH_2 group in PVDF and the -NH_2 group in HHE, and the negatively charged -CF_2 group in PVDF and the -OH group in HHE will all repel. The creation of the β phase will occur because of the consistent PVDF chain orientation under the combined influence of the NH_2-CF_2 dipole and repulsive force. After soaking in ethanol, the PVDF surface's positive group is activated, which facilitates binding to negatively charged groups (Fig. 2h). The activated PVDF was immersed in $HAuCl_4$ solution, and the $AuCl_4^-$ ions had electrostatic adsorption with the PVDF surface. Ultimately, by immersing sodium borohydride, the $AuCl_4^-$ ions adsorbed on the PVDF surface were converted to Au seed. The acetonitrile and Ag^+ have a coordination effect during *in situ* growth with growth solution, which lessens the self-nucleation phenomena. As shown in reaction system constituted by acetonitrile, ethanol, PVP, $AgNO_3$ and ascorbic acid (Fig. 2i), with the Au seed serving as the site of nucleation, the stable and evenly distributed Ag nano-monomers would progressively accumulate on the PVDF surface. Furthermore, we were shocked to learn that the PVDF surface's hydrophilicity improves when it becomes plasma functionalized (Fig. 2g, h, i and Fig. S7), which is advantageous for the adsorption detection of liquid human secretions.

2.2. *Multifunctional sensing for biomechanics and biomolecules employing the PVDF@Ag fiber*

Wearable health monitoring by integrated biomechanics and biomolecule sensing via clothes carrier is a workable approach. PVDF@Ag nanofiber has the potential to combine SERS detection and piezo-response mechanisms. First, the piezoelectric response was used to study the biomechanics monitoring mechanism (Fig. 3a). Fig. 3b and Fig. 3c display the piezoelectric outputs at various intensities and frequencies. The output voltage rises from 2 V to 4 V in proportion to the rising impact frequency. There is a good linear relationship between the pressure and the output voltage and current, which both climb with increasing pressure.

As shown in Fig. S8, the segmented linear relationships between voltage and pressures are located at the range of 0–10 Kpa, 10–30 Kpa and 30–120 KPa. It turns out that the sensitivity value of S is 0.49 KPa^{-1}, 0.09 KPa^{-1}, 0.01 KPa^{-1} and the linearity value of R^2 is 0.9857, 0.9335, 0.9999 at the range of 0–10 KPa, 10–30 Kpa and 30–120 KPa respectively; The sensitivity of pressure response was to 155 ms (Fig. S9). PVDF@Ag membrane contacted by polyimide film (Fig. S10-S12) was subjected to 60 N of force and 0.25–1.33 Hz of frequency during testing. The output current rises from 1 nA to 6 nA as the impact frequency

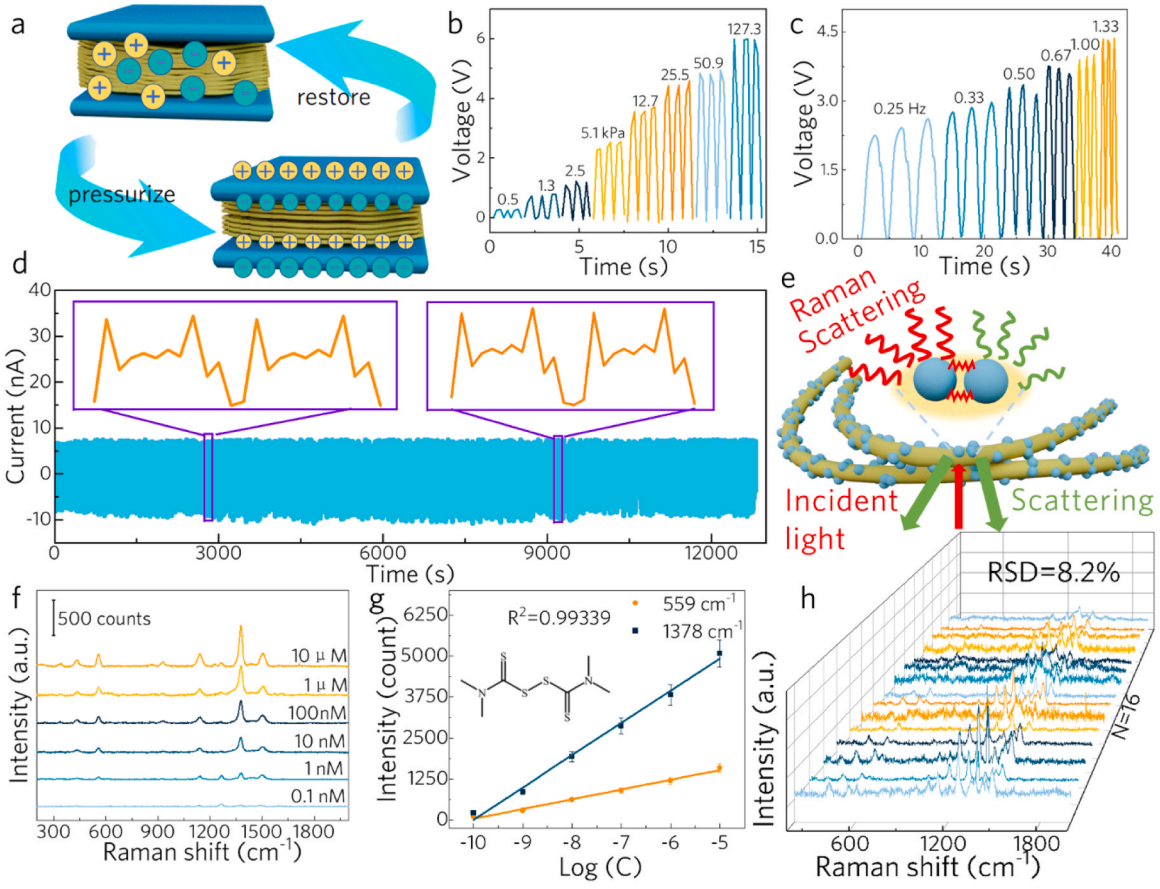


Fig. 3. (a) Schematic diagram of the working principle of PVDF for piezoelectric sensing; Piezoelectric output voltage at different (b) pressures and (c) frequencies; (d) The durability of piezoelectric output after continuous cycles; (e) Schematic diagram of SERS detection of biomolecules by PVDF@Ag fiber; (f) SERS spectra of thiram at different concentrations detected by PVDF@Ag; (g) Linear calibration plot between SERS intensity and concentration; (h) SERS spectra of thiram obtained at 16 spots from surface of PVDF@Ag fiber.

increases (Fig. S13 and S14). After 7000 continuous loading cycles at a pressure of 5 KPa, the current nearly stays constant, and the enlarged views further show the stable sensing current (Fig. 3d). In order to evaluate the SERS performance of PVDF@Ag fiber (Fig. 3e), the SERS signals of thiram molecules adsorbed on the surface of PVDF@Ag are collected (Fig. 3f, g and h) and (Table S1). The linear calibration plot between the signal intensity and thiram concentration at 1378 and 559 cm^{-1} is shown in Fig. 3f and g, and the LOD is 0.1 nM. According to the statistic of thiram peaks at 1378 cm^{-1}, the calculated relative standard deviation (RSD) is 8.2 % (Fig. 3h). PVDF@Ag fiber's method of action allows it to detect multimodal signals by sensing biomechanics and biomolecules.

2.3. PVDF@Ag fiber's biomimetic helix for obtaining a steady SERS signal

Biomolecules serve as a crucial source of health data for wearable sensing. One potential mediator to close the gap between biomechanics and biomolecule sensing is PVDF@Ag. The primary problem for wearable SERS sensing is mechanical robustness under deformation. How to keep the signal stable and sensitive is a major difficulty. The PVDF@Ag twisted fiber was created to reduce the impact of cutaneous deformation. (Fig. 4a_1–a_4), Fig. 4a_5 also displays a high-resolution TEM image and a microscopic view of the PVDF and Ag contact. The PVDF@Ag fiber's biomimetic helix was attracted to the butterfly's detecting antennae shown in Fig. 4b. Twisting is a densification process that may, in fact, enhance hotspot densities at the macroscale (Fig. 4c, d and Fig. S15), but this density gain is minimal at the nanoscale. The main cause of the signal attenuation of the PVDF@Ag membrane without twist may be the increase in fiber distance of the membrane under tensile deformation, which usually produce void (Fig. 4e), and these voids are usually larger than the diameter of the spot of excitation light during the SERS detection (Fig. S16), which is the main factor leading to an attenuation of SERS signal. As shown in Fig. 4f, the SERS signal of twisted fiber of PVDF@Ag remained stable at 50 % strain. On the other hand, upon tensile deformation, the SERS activity started to decrease for the PVDF@Ag membrane without the twist. Therefore, the greatest significance of twisting is to resist signal attenuation caused by tensile deformation. We also noticed that even after 1000 cycles of stretching and relaxing (~10 % strain; Fig. 4g), the SERS activity remained consistent. Then, compact layers of twisted fibers might withstand the SERS signal's decline during the deformation [23,33,34,39]. The fibrous membrane of PVDF@Ag was fitted onto fabric to improve comfort and utility. Fig. 4h–i displays optical images of PVDF@Ag twisted fiber put on clothing, demonstrating how the material responds to deformations caused by human motion. The PVDF@Ag fiber replicated the skin's normal deformations in every instance. Above all, PVDF@Ag fiber offers an integrated platform for wearable sensor implementation over an extended length of time. Nonetheless, PVDF@Ag twisted fiber offers beneficial anti-interference when worn as part of a clothing carrier for

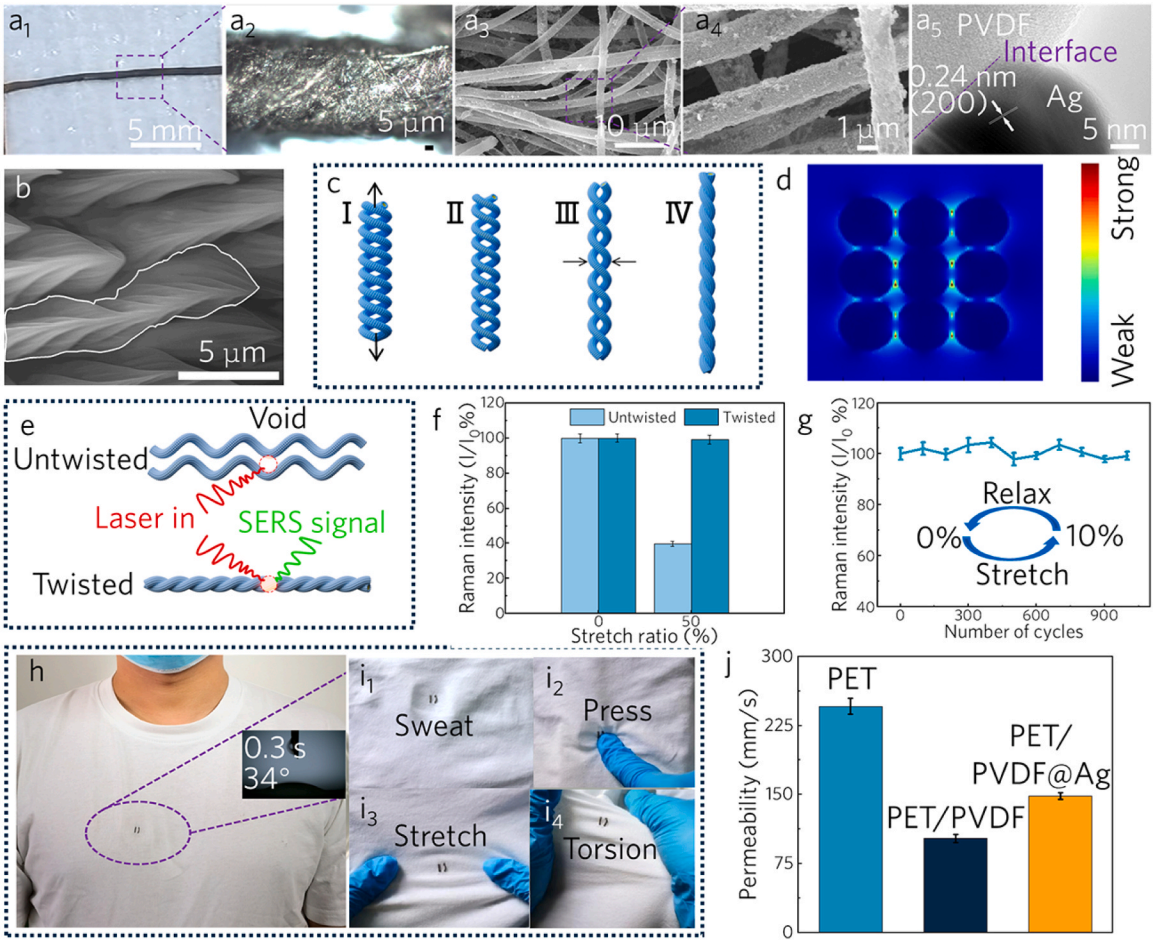


Fig. 4. (a_1-a_4) The twisted fiber of PVDF@Ag from optical microscopic amplification to electron microscopic amplification; (a_5) High-resolution TEM image of the interface of PVDF@Ag; (b) Microstructure of butterfly antennae; (c) Stretch process of twisted fiber; (d) Simulation of localized surface plasmon resonance for twisted fiber during the SERS sensing; (e) Stretch process of untwisted fibers, which usually produce void; (f) SERS responses of the twisted fiber of PVDF@Ag and untwisted fiber membrane under deformations; (g) Characteristics of the stability of SERS signal after the cyclic stretching test; (h) Hygroscopicity and (i) tensile test of the twisting fiber of PVDF@Ag integrated on clothing carrier; (j) Breathability of fibrous membranes of PVDF@Ag integrated by PET fabric.

wearable sensing. Additionally, during wearable application, the fibrous membranes of PVDF@Ag integrated by polyester (PET) fabric demonstrate excellent moisture absorption (Fig. 4h), air permeability (Fig. 4j), and antibacterial capacity (Fig. S17).

2.4. Wearable sensing-based multimodal analysis for biomechanics and biomolecules

One important indicator of health status is biomechanics and biometabolites . Fig. 5a–c depict similar signals of letter sounds (X, P, and U), muscular movement, nose breathing, and mouth breathing. These signals clearly differ from one another and are useful for the early detection of neuropathic disease. Furthermore, wearable SERS detection of secretory chemicals during sweat and respiration would have a beneficial application for healthcare management with the shrinking of the Raman spectrometer (Fig. S18). The greatest significance of twisting is to resist signal attenuation caused by tensile deformation. Then the better signal output of SERS could be realized. Sweat and respiratory secretions are noninvasive biomarkers that can be gathered for medical evaluation. Here, we used SERS detection to gather sweat from six volunteers (Fig. 5d–f), and the primary feature peaks that were found were 552, 607, 829, 886, 1003, 1052, 1081, 1115, 1272, 1415, 1451, and 1553 cm^{-1} (Table S2). Specifically, Raman shifts of 552, 1003, 1115, 1415 and 1553 cm^{-1} represent the ν(NCO), ν(CN), $\rho(NH_2)$, s(CN), and v (CO) of urea [40,41], respectively; urea is the main nitrogen-containing product of protein metabolism. Higher urea will increase the discharge burden of the kidney, resulting in renal function. Based on our analysis for SERS spectra of secretions at sweat (Table S2), 886, 1052 and 1272 cm^{-1} represent the ν(CC), δ(CH), and Amid III, of the proteins [41];1081 and 1451 cm^{-1} represent ν(C-O), δ(C-COH) [40] and δ(C-H), δ as (CH_3) [41] of lactic acid, respectively; The peak of 607 cm^{-1} belongs to O═C-N- bending (amino acids and proteins) [42]; The peak of 829 cm^{-1} is caused by $\rho(CH_3)$ (amino acid and lactic acid) [41]. We also found differences between volunteers of sweat (Fig. 5e), which opens up the possibility of individual medical monitoring. Real-time sweat secretion monitoring could provide health-related data on wound healing, cystic fibrosis, dehydration, and other conditions [43].

Additionally, we obtained respiratory secretions using SERS testing from four participants (Fig. 5g, h, and Fig. S19) and (Table S3). Raman shifts of 636, 842, 948, 1003, 1022, 1548 and 1601 cm^{-1} are caused by amino acids, which represent C-S stretching vibration (tyrosine) [44], ring breathing mode, C-C stretch of proline ring (tyrosine, proline) [45], v (C-C) (proline) [46,47], vs (C-C) (phenylalanine) [46], δ(C-H) (phenylalanine) [47], ν(C═C) (Typtophan) [46] and C═C in-plane bending mode(phenylalanine, tyrosine) [45]; 1249 and 1581 cm^{-1} represent C-N (xanthine) [48,49] and C-N (hypoxanthine) [48], respectively; The 725 cm^{-1} peak belongs to δ (C-H) (adenine and coenzyme A) [45], the peak of 1454 cm^{-1} belongs to C-N or C-C, CH_2 bending mode of proteins (hypoxanthine, protein, phenylalanine) [45], and the peak of 1637 cm^{-1} is attributed to Amid I (protein) [48]. As the sweat secretions, the difference between volunteers was also found, and the SERS signals at different positions of PVDF@Ag fiber also show the dissimilarity, which further illustrates the diversity of respiratory secretions (Fig. 5h and Fig. S19). Therefore, wearable detection technology for multimodal biomechanics and biomolecule sensing may find an

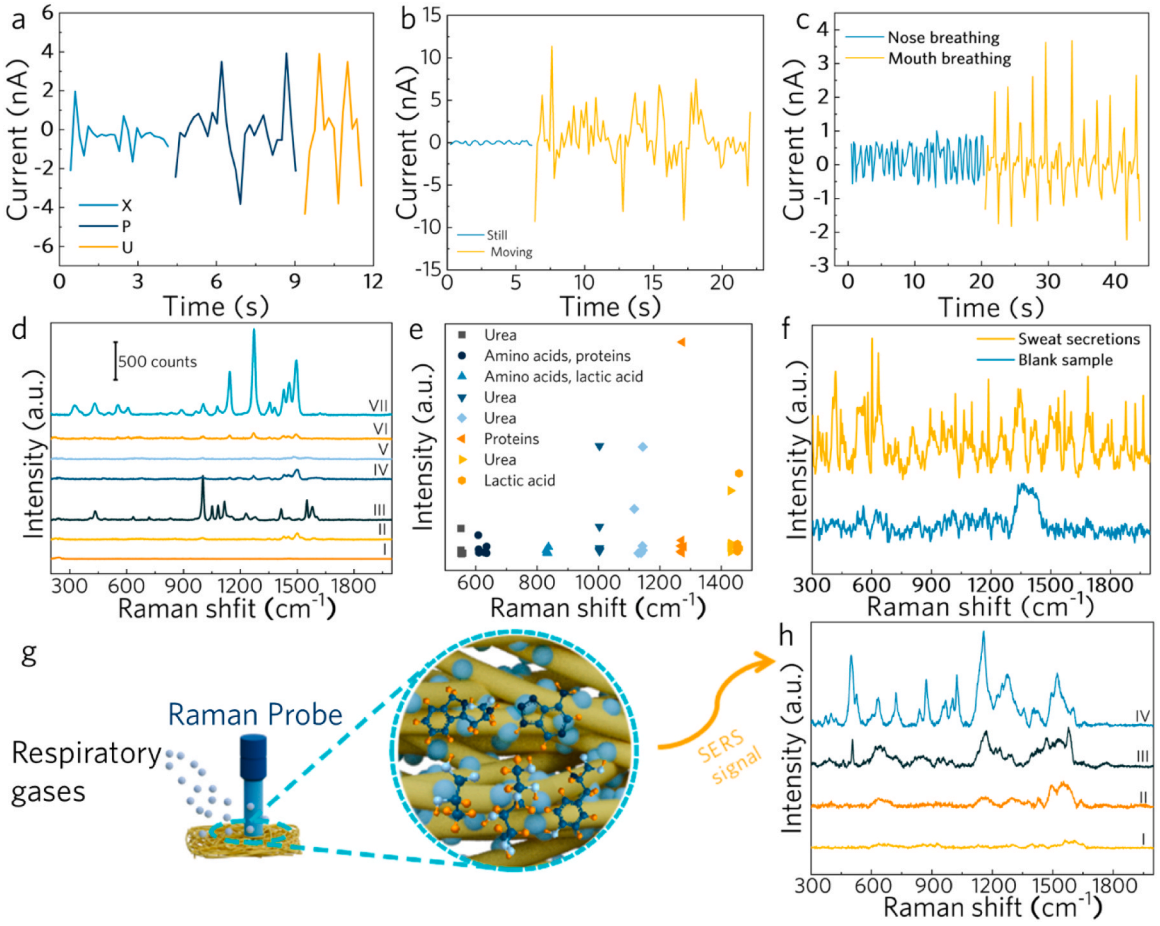


Fig. 5. (a) Similar signals of letter sound X, P and U; (b) muscle fremitus, (c) nose breathing and mouth breathing; (d) SERS spectra of secretions in sweat from six volunteers (II-VII); (e) Statistics of sweat secretions based on the SERS spectrum collected; (f) Sweat secretions collected by handheld Raman spectrometer; (g, h) SERS spectra of secretions in respiration from 4 volunteers.

application in the field of health management [48–50].

2.5. *Wearable electronics integrated by deep-learning arithmetic-assisted health assessment*

Wearable bioelectronics have found a convenient platform in textiles for sensors [13,51–53], and it would open the door to healthcare and wearable medication [54,55]. Further-more, a wearable sensor system is built to identify biomechanics, biomolecules, and even health information by combining with the deep-learning technique (Fig. 6a–c). Applications for sensor-based human action recognition (HAR) are numerous and include behavior analysis, tailored treatment, health monitoring, and surveillance systems. Health information identification is complex and requires automated computing [56,57]. Support vector machine (SVM)-based machine learning algorithm is created for HAR. A binary classification model is SVM. Unlike perceptron, its basic model is a linear

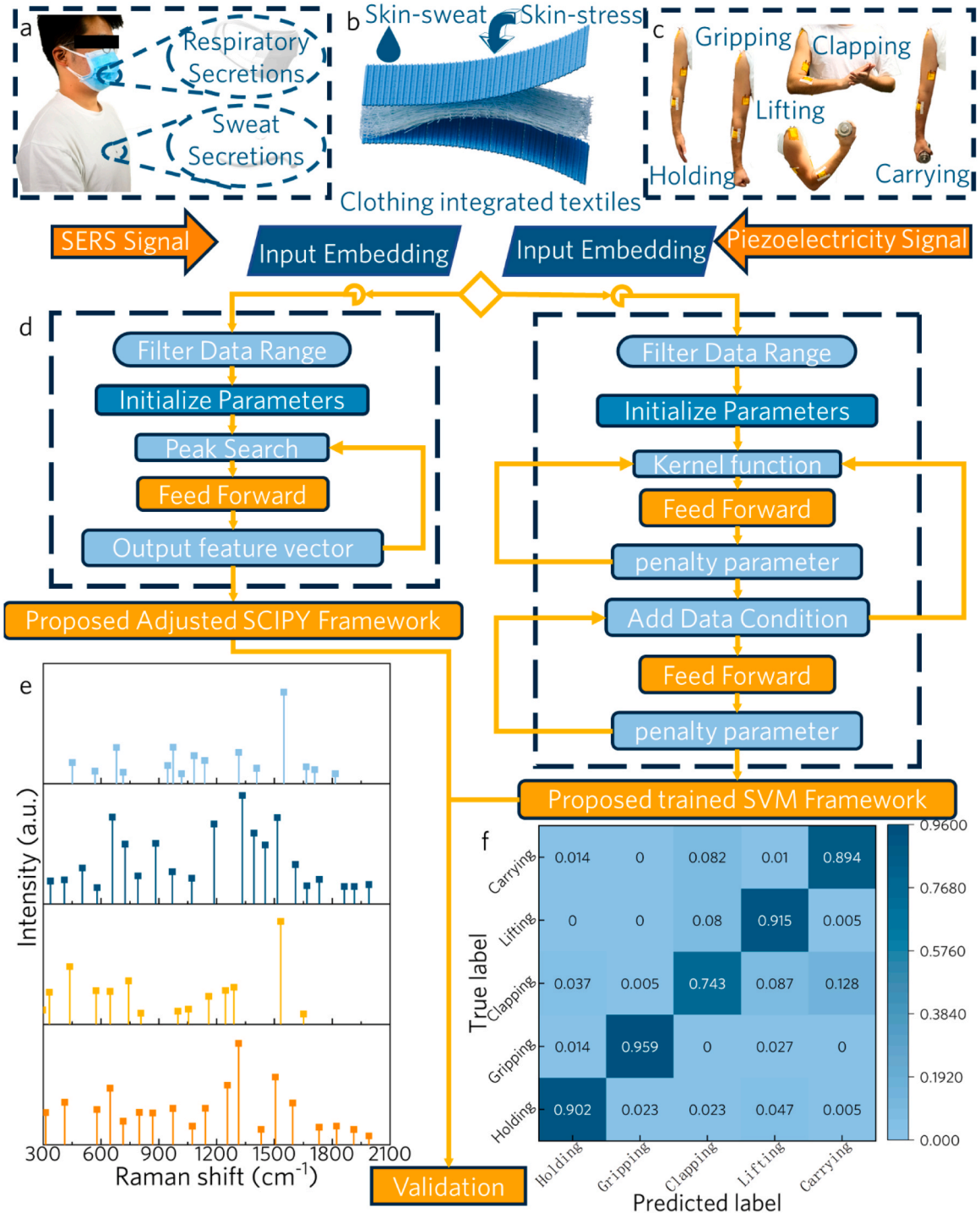


Fig. 6. Textile carriers integrate a machine learning algorithm for wearable health signal monitoring. (a) Analysis of secretions at sweat and respiration; (b) Textile sensor integrated by PVDF@Ag. (c) Fiber membranes of PVDF@Ag fixed to the skin surface to collect muscular action, such as holding, gripping, clapping, lifting, and carrying. (d) The structural construction of the machine learning algorithm; (e) The output results of SERS peaks in respiratory secretion from four volunteers; (f) The confusion matrix for human action-level classification by SVM.

classifier defined in the feature space with the biggest interval. Maximizing the interval is the SVM's learning approach. This can be expressed as a convex quadratic programming problem to be solved, or as the minimization of a regularized hinge loss function. The basic idea of SVM learning is to solve the separation hyperplane that can correctly partition the training data set and has the largest geometric interval. As shown in below, $w{\cdot}x+b=0$ is the separation hyperplane. There are an infinite number of such hyperplanes for linearly separable data sets; however, the separated hyperplane with the biggest geometric interval is unique. We can analyse how far the sample point is from the plane using the hyperplane expression. Suppose $P(X_1, X_2 \ldots X_n)$ is a point in the sample, where *xi* is the characteristic variable. Then the distance from the point to the hyperplane can be calculated with the following formula (1):

$$d = \frac{|w_1^* \times 1 + w_2^* \times 2 + \ldots n^* x_n + b|}{\sqrt{w_1^2 + w_2^2 + \ldots + w_n^2}} = \frac{|W^T{*}X + b|}{\| W \|} \quad (1)$$

Where $\| W \|$ is the norm of the hyperplane, and the b is the intercept in the linear equation.

Fig. 6d shows an SVM unit. It is made up of categories and data that include fundamental elements including feedforward networks, kernel functions, and penalty coefficients. The purpose of these parts is to extract features from signals that can be used to distinguish between distinct signals. Fig. 6e and Fig. 6f provide a statistics list for the actions. Because of the piezoelectric properties of piezoelectric sensors, a significant amount of data that fluctuate close to zero are filtered out of the signals during the data processing stage. And use the grid search method to get the optimal kernel function and penalty parameter. After an extracted data passes through SVM, the category of the action will be predicted, so that the biophysical signals can be recognized. PVDF@Ag membrane was connected to several body areas (Fig. 6c) to serve as a sensor to ''feel'' distinct activities and illustrate the practical usage situations.

Electrical signals that were produced were recorded. For five different human acts, a total of 1050 samples have been gathered. These behaviors can be identified by using vector machines to classify the gathered data. Fig. 6f and Fig. S20 display the testing results' confusion matrix. The prediction precision for five categories (human actions) is 90.2 %, 95.9 %, 74.3 %, 91.5 %, and 89.4 %, respectively (Fig. 6f). With the help of the PVDF@Ag sensor, it is discovered that SVM yields the best kernel function and optimal penalty coefficient, proving its usefulness in HAR. Additionally, Fig. 6e displays the results of the extraction of distinctive peaks from respiratory secretion samples taken from four volunteers. The Raman database is used to validate the peak positions of biomolecules using the ''fingerprint'' method. We believe that our clothing carrier-integrated wearable biomechanics and biomolecule sensing will spark unexpected applications that open up hitherto unexplored possibilities.

3. Conclusions

The initial design of the PVDF@Ag fiber incorporated the LSPR effect with piezoelectricity. A PVDF core@Ag shell structure is created when compact and homogenous AgNPs are *in-situ* grown on high-curvature PVDF fibers by reducing the reduction potential of Ag^+ ions and inhibiting self-nucleation. A twisted fiber of PVDF@Ag is created by rolling and twisting the fibrous membrane. Since the twisted fiber maintains its stability while stretched, voids can be successfully avoided. Twisted fibers' compactness allows for the surface of the fibers to be stimulated by excitation light, preventing the SERS signal from being attenuated during wearable detection due to tensile deformation. To identify the output signal of the PVDF@Ag sensing fiber, HAR has developed a deep neural network based on SVM. A precision rate of 88.0 % for five kinds of similar motions was obtained. Furthermore, PVDF@Ag was able to achieve noninvasive secretion extraction and recognition in sweat and respiration based on the SERS ''fingerprint'' spectra. Additionally, research is done on the relationship between the output spectrum and physiological data from the human body. Nonetheless, the PVDF@Ag fiber uses a textile carrier to bridge the sensing gap between biomechanics and biomolecule. Such integrated and multimodal signal analysis could mark a significant advancement in wearable health monitoring with the development of the next generation of wearable sensors.

4. Experimental section

4.1. Chemicals and materials

All reagents are analytical grade and have not been further purified. Polyvinylidene fluoride (DS204) was purchased from Shandong Dongyue Shenzhou New Materials Co., Ltd., N,N-dimethylformamide (DMF) and acetonitrile were purchased from Tianjin Fuyu Fine Chemical Co., Ltd., hydroxylamine hydrochloride (HHE) was purchased from Tianjin Damao Chemical Reagent Factory, $HAuCl_4$ was purchased from Shanghai Chemical Reagent Factory, polyvinylpyrrolidone (PVP) and ascorbic acid (AA) were purchased from Aladdin Reagent Co., Ltd. Sodium borohydride ($NaBH_4$) was purchased from Chengdu Cologne Chemicals Co., Ltd., silver nitrate ($AgNO_3$) was purchased from Shanghai Institute of Fine Chemical Materials, and absolute ethanol was purchased from Hengxing reagent. The sweat came from six volunteers with consent, and did not involve any ethical issues or private information.

4.2. Characterization

The samples were characterized by using a field-emission scanning electron microscope (Quanta-450-FEG) and EDS (X-MAX50). The XRD mode was obtained using a diffractor DX-2700BH. The Fourier transform infrared spectrometer (Type Nicolet is50) was used. UV–visible spectroscopy was performed using a Shimadzu UV-2600 spectrophotometer. Type JC2000C1 of contact angle meter (Shanghai Zhongchen Digital Technology Equipment Co., Ltd.) is used to test the contact angle. The Raman spectra were recorded using a laser Raman spectrometer (HORIBA, LabRAM HR evolution) and a handheld Raman spectrometer (Optosky ART6500). Piezoelectric testing was performed using the Keithley2410.

4.3. Preparation of PVDF/HHE nanofiber membranes

Mixing PVDF (12 % by the total weight) with hydroxylamine hydrochloride (2 % of PVDF mass), dissolving DMF and acetone solvent with a mass ratio of 5:5, and stirring in a water bath at 60 °C. After the 6 h of stirring, an electrospinning solution is prepared. Then the PVDF nanofiber membrane was obtained by spinning at a voltage of 18 KV, a liquid inlet speed of 1 mL/h, a speed of 300 r·min^{-1} and a spacing of 15 cm. Dry the PVDF membrane for further use. All experimental steps are performed under ambient atmospheric conditions.

4.4. Preparation of PVDF@Au seed

The nanofiber membrane was placed in absolute ethanol for a few seconds, then soaked in chloroauric acid (0.02 M) for one minute, washed off the surface with deionized water after removal, and put it into sodium borohydride (0.02 M) for one minute. After taking it out, washing it in deionized water and soaking it in absolute ethanol. Obtaining the PVDF@Au seed nanofiber membrane with 2,4,6,8 cycles.

4.5. Preparation of PVDF@Ag nanofiber membranes

A certain amount of PVP (5 wt%), acetonitrile, ethanol, $AgNO_3$ (0.1 M) and ascorbic acid (0.1 M) were added to the deionized water. At

10 °C, the PVDF@Au seed nanofiber membrane was added to the growth solution for vigorous agitation. PVDF@Ag nanofiber membranes were obtained after 2,4,6 cycles. The PVDF@Ag nanofiber membranes were washed with deionized water and dried at room temperature.

4.6. Preparation of piezoelectric membrane of PVDF@Ag

Using aluminum foil as the upper and lower electrodes of the piezoelectric sensor, a sandwich structure is formed. The wires are led out on the aluminum foil and encapsulated with insulated polyimide (PI) tape to obtain a piezoelectric sensor.

4.7. Preparation of twisted fiber of PVDF@Ag

A torsional force was applied to twist the PVDF@Ag nanofiber membrane and the shape was fixed, in which a signal-stable SERS substrate of twisted fiber of PVDF@Ag was obtained.

Supporting information

Supplementary Figure, Data and Statement are of included.

CRediT authorship contribution statement

Tao Fu: Formal analysis. **Xiaoming Wu:** Supervision. **Xinhai He:** Project administration. **Liangjun Xia:** Visualization. **Yang Li:** Software, Investigation. **Jianzhao Gao:** Software. **Meng Zhang:** Formal analysis. **Junhao Liang:** Resources. **Weilin Xu:** Resources, Funding acquisition. **Dongzhen Chen:** Writing – original draft, Funding acquisition, Data curation.

Declaration of Competing Interest

The authors declare that they have no known competing financial interests or personal relationships that could have appeared to influence the work reported in this paper.

Data Availability

Data will be made available on request.

Acknowledgments

This work was supported by the National Key Research and Development Program of China (Grant No. 2022YFB3805800), "Textile Vision" Applied Basic Research of China National Textile and Apparel Council (No. J202303), the Xi'an Science and Technology Project (No. 22GXFW0035), the Scientific Research Program Funded by Shaanxi Provincial Education Department (No. 23JK0465), the project of Sports Bureau of Shaanxi Province (No. 2023053). The authors thank Rui Gao from Optosky for helping us to complete the Hand-held Raman detection.

Appendix A. Supporting information

Supplementary data associated with this article can be found in the online version at doi:10.1016/j.nanoen.2024.109821.

References

[1] J.W. Gao, Y.B. Fan, Q.T. Zhang, L. Luo, X.Q. Hu, Y. Li, J.C. Song, H.J. Jiang, X. Y. Gao, L. Zheng, W. Zhao, Z.H. Wang, W. Ai, Y. Wei, Q.B. Lu, M.Z. Xu, Y.T. Wang, W.T. Song, X.W. Wang, W. Huang, Ultra-robust and extensible fibrous mechanical sensors for wearable smart healthcare, Adv. Mater. 34 (2022) 2107511, https://doi.org/10.1002/adma.202107511.

[2] N.J. Schork, Personalized medicine: time for one-person trials, Nature 520 (2015) 609–611, https://doi.org/10.1038/520609a.

[3] C.H. Wang, X.S. Li, H.J. Hu, L. Zhang, Z.L. Huang, M.Y. Lin, Z.R. Zhang, Z.N. Yin, B. Huang, H. Gong, S. Bhaskaran, Y. Gu, M. Makihata, Y.X. Guo, Y.S. Lei, Y. M. Chen, C.F. Wang, Y. Li, T.J. Zhang, Z.Y. Chen, A.P. Pisano, L.F. Zhang, Q. F. Zhou, S. Xu, Monitoring of the central blood pressure waveform via a conformal ultrasonic device, Nat. Biomed. Eng. 2 (2018) 687–695, https://doi.org/10.1038/s41551-018-0287-x.

[4] H.H. Shi, Y.F. Pan, L. Xu, X.M. Feng, W.Y. Wang, P. Potluri, L.B. Hu, T. Hasan, Y.Y. S. Huang, Sustainable electronic textiles towards scalable commercialization, Nat. Mater. 22 (2023) 1294–1303, https://doi.org/10.1038/s41563-023-01615-z.

[5] M. Chen, P. Li, R. Wang, Y.Z. Xiang, Z.H. Huang, Q. Yu, M.Y. He, J. Liu, J.X. Wang, M.Y. Su, M.N. Zhang, A.J. Jian, J.Y. Ouyang, C.X. Zhang, J. Li, M.X. Dong, S. N. Zeng, J.W. Wu, P. Hong, C. Hou, N. Zhou, D.Y. Zhang, H.M. Zhou, G.M. Tao, Multifunctional fiber-enabled intelligent health agents, Adv. Mater. 34 (2023) 2200985, https://doi.org/10.1002/adma.202200985.

[6] A.D. Mickle, S.M. Won, K.N. Noh, J. Yoon, K.W. Meacham, Y.G. Xue, L. A. McIlvried, B.A. Copits, V.K. Samineni, K.E. Crawford, D.H. Kim, P. Srivastava, B. H. Kim, S. Min, Y. Shiuan, Y. Yun, M.A. Payne, J.P. Zhang, H. Jang, Y.H. Li, H. H. Lai, Y.G. Huang, S.I. Park, R.W. Gereau, J.A. Rogers, A wireless closed-loop system for optogenetic peripheral neuromodulation, Nature 565 (2019) 361–365, https://doi.org/10.1038/s41586-018-0823-6.

[7] J.L. Zhang, T. Yang, G. Tian, B.L. Lan, W.L. Deng, L.H. Tang, Y. Ao, Y. Sun, W. H. Zeng, X.R. Ren, Z.Y. Li, L. Jin, W.Q. Yang, Spatially confined MXene/PVDF nanofiber piezoelectric electronics, Adv. Fiber Mater. 6 (2023) 133–144, https://doi.org/10.1007/s42765-023-00337-w.

[8] M.D. Han, H.L. Wang, Y.Y. Yang, C.M. Liang, W.B. Bai, Z. Yan, H.B. Li, Y.G. Xue, X. L. Wang, B. Akar, H.B. Zhao, H.W. Luan, J. Lim, I. Kandela, G.A. Ameer, Y. H. Zhang, Y.G. Huang, J.A. Rogers, Three-dimensional piezoelectric polymer microsystems for vibrational energy harvesting, robotic interfaces and biomedical implants, Nat. Electron. 2 (2019) 26–35, https://doi.org/10.1038/s41928-018-0189-7.

[9] P.F. Zhao, Y.L. Song, P. Xie, F. Zhang, T. Xie, G. Liu, J.Y. Zhao, S.T. Han, Y. Zhou, All-organic smart textile sensor for deep-learning-assisted multimodal sensing, Adv. Funct. Mater. 33 (2023) 2301816, https://doi.org/10.1002/adfm.202301816.

[10] Y.C. Cai, J. Shen, G. Ge, Y.Z. Zhang, W.Q. Jin, W. Huang, J.J. Shao, J. Yang, X. C. Dong, Stretchable $Ti_3C_2T_x$ MXene/carbon nanotube composite based strain sensor with ultrahigh sensitivity and tunable sensing range, ACS Nano 12 (2018) 56–62, https://doi.org/10.1021/acsnano.7b06251.

[11] K.W. Zeng, X. Shi, C.Q. Tang, T. Liu, H.S. Peng, Design, fabrication and assembly considerations for electronic systems made of fibre devices, Nat. Rev. Mat. 8 (2023) 552–561, https://doi.org/10.1038/s41578-023-00573-x.

[12] W. Gao, S. Emaminejad, H.Y.Y. Nyein, S. Challa, K.V. Chen, A. Peck, H.M. Fahad, H. Ota, H. Shiraki, D. Kiriya, D.H. Lien, G.A. Brooks, R.W. Davis, A. Javey, Fully integrated wearable sensor arrays for multiplexed *in situ* perspiration analysis, Nature 529 (2016) 509–514, https://doi.org/10.1038/nature16521.

[13] W.C. Chen, W. Fan, Q. Wang, X.C. Yu, Y. Luo, W.T. Wang, R.X. Lei, Y. Li, A nano-micro structure engendered abrasion resistant, superhydrophobic, wearable triboelectric yarn for self-powered sensing, Nano Energy 103 (2022) 107769,, https://doi.org/10.1016/j.nanoen.2022.107769.

[14] E. Garcia-Cordero, F. Bellando, J.R. Zhang, F. Wildhaber, J. Longo, H. Guérin, A. M. Ionescu, Three-dimensional integrated ultra-low-volume passive microfluidics with ion-sensitive field-effect transistors for multiparameter wearable sweat analyzers, ACS Nano 12 (2018) 12646–12656, https://doi.org/10.1021/acsnano.8b07413.

[15] W. Gao, H.Y.Y. Nyein, Z. Shahpar, H.M. Fahad, K. Chen, S. Emaminejad, Y.J. Gao, L.C. Tai, H. Ota, E. Wu, J. Bullock, Y.P. Zeng, D.H. Lien, A. Javey, Wearable microsensor array for multiplexed heavy metal monitoring of body fluids, ACS Sens. 1 (2016) 866–874, https://doi.org/10.1021/acssensors.6b00287.

[16] H.Y.Y. Nyein, W. Gao, Z. Shahpar, S. Emaminejad, S. Challa, K. Chen, H.M. Fahad, L.C. Tai, H. Ota, R.W. Davis, A. Javey, A wearable electrochemical platform for noninvasive simultaneous monitoring of Ca^{2+} and pH, ACS Nano 10 (2016) 7216–7224, https://doi.org/10.1021/acsnano.6b04005.

[17] H. Lee, T.K. Choi, Y.B. Lee, H.R. Cho, R. Ghaffari, L. Wang, H.J. Choi, T.D. Chung, N.S. Lu, T. Hyeon, S.H. Choi, D.H. Kim, A graphene-based electrochemical device with thermoresponsive microneedles for diabetes monitoring and therapy, Nat. Nanotechnol. 11 (2016) 566–572, https://doi.org/10.1038/nnano.2016.38.

[18] S. Nakata, M. Shiomi, Y. Fujita, T. Arie, S. Akita, K. Takei, A wearable pH sensor with high sensitivity based on a flexible charge-coupled device, Nat. Electron. 1 (2018) 596–603, https://doi.org/10.1038/s41928-018-0162-5.

[19] Y.J. Hong, H. Lee, J. Kim, M. Lee, H.J. Choi, T. Hyeon, D.H. Kim, Multifunctional wearable system that integrates sweat-based sensing and vital-sign monitoring to estimate pre-/post-exercise glucose levels, Adv. Funct. Mater. 28 (2018) 1805754, https://doi.org/10.1002/adfm.201805754.

[20] J. Kim, J.R. Sempionatto, S. Imani, M.C. Hartel, A. Barfidokht, G.D. Tang, A. S. Campbell, P.P. Mercier, J. Wang, Simultaneous monitoring of sweat and interstitial fluid using a single wearable biosensor platform, Adv. Sci. 5 (2018) 1800880,, https://doi.org/10.1002/advs.201800880.

[21] A. Martín, J. Kim, J.F. Kurniawan, J.R. Sempionatto, J.R. Moreto, G.D. Tang, A. S. Campbell, A. Shin, M.Y. Lee, X.F. Liu, J. Wang, Epidermal microfluidic electrochemical detection system: enhanced sweat sampling and metabolite detection, ACS Sens. 2 (2017) 1860–1868, https://doi.org/10.1021/acssensors.7b00729.

[22] D.Z. Chen, T.S. Chen, Y. Li, S.X. Li, L. Zhang, Y.W. Ren, Y.W. Wang, J.H. Liang, T. Fu, M. Zhang, X.H. He, A flexible sensor based on 3D gold@carbonaceous nanohybrid with defect sites of conductivity for the wearable sensing at low stress, Nano 16 (2021) 2150044, https://doi.org/10.1142/S1793292021500442.

[23] D.Z. Chen, L. Zhang, P. Ning, H.Z. Yuan, Y. Zhang, M. Zhang, T. Fu, X.H. He, *In-situ* growth of gold nanoparticles on electrospun flexible multilayered PVDF nanofibers for SERS sensing of molecules and bacteria, Nano Res. 14 (2021) 4885–4893, https://doi.org/10.1007/s12274-021-3530-9.
[24] B. Sun, Y.Z. Long, Z.J. Chen, S.L. Liu, H.D. Zhang, J.C. Zhang, W.P. Han, Recent advances in flexible and stretchable electronic devices *via* electrospinning, J. Mater. Chem. C 2 (2014) 1209–1219, https://doi.org/10.1039/C3TC31680G.
[25] I.H. Kim, S. Choi, J. Lee, J. Jung, J. Yeo, J.T. Kim, S. Ryu, S.K. Ahn, J. Kang, P. Poulin, S.O. Kim, Human-muscle-inspired single fibre actuator with reversible percolation, Nat. Nanotechnol. 17 (2022) 1198–1205, https://doi.org/10.1038/s41565-022-01220-2.
[26] T. Yang, H. Yang, S.J. Zhen, C.Z. Huang, Hydrogen-bond-mediated *in situ* fabrication of AgNPs/Agar/PAN electrospun nanofibers as reproducible SERS substrates, ACS Appl. Mater. Interfaces 7 (2015) 1586–1594, https://doi.org/10.1021/am507010q.
[27] M. Chung, W.H. Skinner, C. Robert, C.J. Campbell, R.M. Rossi, V. Koutsos, N. Radacsi, Fabrication of a wearable flexible sweat ph sensor based on SERS-active Au/TPU electrospun nanofibers, ACS Appl. Mater. Interfaces 13 (2021) 51504–51518, https://doi.org/10.1021/acsami.1c15238.
[28] W. Fan, R.X. Lei, H. Dou, Z. Wu, L.L. Lu, S.J. Wang, X.Q. Liu, W.C. Chen, M. Rezakazemi, T.J.M. Aminabhavi, Y. Li, S.B. Ge, Sweat permeable and ultrahigh strength 3D PVDF piezoelectric nanoyarn fabric strain sensor, Nat. Commun. 15 (2024) 3059, https://doi.org/10.1038/s41467-024-47810-7.
[29] T. Li, Z.Q. Feng, M.H. Qu, K. Yan, T. Yuan, B.B. Gao, T. Wang, W. Dong, J. Zheng, Core/shell piezoelectric nanofibers with spatial self-orientated β-phase nanocrystals for real-time micropressure monitoring of cardiovascular walls, ACS Nano 13 (2019) 10062–10073, https://doi.org/10.1021/acsnano.9b02483.
[30] S. Cheon, H. Kang, H. Kim, Y. Son, J.Y. Lee, H.J. Shin, S.W. Kim, J.H. Cho, High-performance triboelectric nanogenerators based on electrospun polyvinylidene fluoride-silver nanowire composite nanofibers, Adv. Funct. Mater. 28 (2017) 1703778,, https://doi.org/10.1002/adfm.201703778.
[31] M. Chen, J.Y. Ouyang, A.J. Jian, J. Liu, P. Li, Y.X. Hao, Y.C. Gong, J.Y. Hu, J. Zhou, R. Wang, J.X. Wang, L. Hu, Y.W. Wang, J. Ouyang, J. Zhang, C. Hou, L. Wei, H. H. Zhou, D.Y. Zhang, G.M. Tao, Imperceptible, designable, and scalable braided electronic cord, Nat. Commun. 13 (2022) 7097, https://doi.org/10.1038/s41467-022-34918-x.
[32] Y.L. Wang, C. Zhao, J.J. Wang, X. Luo, L.J. Xie, S.J. Zhan, J.M. Kim, X.Z. Wang, X. J. Liu, Y.B. Ying, Wearable plasmonic-metasurface sensor for noninvasive and universal molecular fingerprint detection on biointerfaces, Sci. Adv. 7 (2021), https://doi.org/10.1126/sciadv.abe4553.
[33] D.Z. Chen, Z.X. Song, F. Chen, J. Huang, J. Wei, Y.X. Zhao, Simply controllable growth of single crystal plasmonic Au-Ag nano-spines with anisotropic multiple sites for highly sensitive and uniform surface-enhanced Raman scattering sensing, RSC Adv. 6 (2016) 66056–66065, https://doi.org/10.1039/C6RA13420C.
[34] D.Z. Chen, X.D. Zhu, J. Huang, G. Wang, Y. Zhao, F. Chen, J. Wei, Z.X. Song, Y. X. Zhao, Polydopamine@Gold nanowaxberry enabling improved SERS sensing of pesticides, pollutants, and explosives in complex samples, Anal. Chem. 90 (2018) 9048–9054, https://doi.org/10.1021/acs.analchem.8b01348.
[35] T. Yang, H. Pan, G. Tian, B.B. Zhang, D. Xiong, Y.Y. Gao, C. Yan, X. Chu, N.J. Chen, S. Zhong, L. Zhang, W.L. Deng, W.Q. Yang, Hierarchically structured PVDF/ZnO core-shell nanofibers for self-powered physiological monitoring electronics, Nano Energy 72 (2020) 104706, https://doi.org/10.1016/j.nanoen.2020.104706.
[36] T. Huang, S.W. Yang, P. He, J. Sun, S. Zhang, D.D. Li, Y. Meng, J.S. Zhou, H. X. Tang, J.R. Liang, G.Q. Ding, X.M. Xie, Phase-separation-induced PVDF/graphene coating on fabrics toward flexible piezoelectric sensors, ACS Appl. Mater. Interfaces 10 (2018) 30732–30740, https://doi.org/10.1021/acsami.8b10552.
[37] D.Z. Chen, P. Ning, Y. Zhang, J.Y. Jing, M. Zhang, L. Zhang, J. Huang, X.H. He, T. Fu, Z.X. Song, G.Y. He, D. Qian, X.D. Zhu, Ta @Ag porous array with high stability and biocompatibility for SERS sensing of bacteria, ACS Appl . Mater. Interfaces 12 (2020) 20138–20144, https://doi.org/10.1021/acsami.0c03630.
[38] S.K. Karan, R. Bera, S. Paria, A.K. Das, S. Maiti, A. Maitra, B.B. Khatua, An Approach to Design Highly Durable Piezoelectric Nanogenerator Based on Self-Poled PVDF/AlO-rGO Flexible Nanocomposite with High Power Density and Energy Conversion Efficiency, Adv. Energy Mater. 6 (2016) 1601016, https://doi.org/10.1002/aenm.201601016.
[39] V. Sikirzhytski, A. Sikirzhytskaya, I.K. Lednev, Multidimensional Raman spectroscopic signature of sweat and its potential application to forensic body fluid identification, Anal. Chim. Acta 718 (2012) 78–83, https://doi.org/10.1016/j.aca.2011.12.059.
[40] M. Pecul, A. Rizzo, J. Leszczynski, Vibrational Raman and Raman optical activity spectra of d-lactic acid, d-lactate, and d-glyceraldehyde: ab initio calculations, J. Phys. Chem. 106 (2002) 11008–11016, https://doi.org/10.1021/jp021030m.
[41] G. Socrates, Infrared and Raman characteristic group frequencies: tables and charts, Colloid Polym. Sci. 283 (2004) 235. ⟨https://doi.org/10.1007/s00396-004-1164-6⟩.
[42] V.C. Diculescu, M. Beregoi, A. Evanghelidis, R.F. Negrea, N.G. Apostol, I. Enculescu, Palladium/palladium oxide coated electrospun fibers for wearable sweat pH-sensors, Sci. Rep. 9 (2019) 8902, https://doi.org/10.1038/s41598-019-45399-2.
[43] S.F. Qiu, Y.J. Xu, L.L. Huang, W. Zheng, C.B. Huang, S.H. Huang, J.Y. Lin, D. Lin, S. Y. Feng, R. Chen, J.J. Pan, Non-invasive detection of nasopharyngeal carcinoma using saliva surface-enhanced Raman spectroscopy, Oncol. Lett. 11 (2016) 884–890, https://doi.org/10.3892/ol.2015.3969.
[44] K. Qian, Y. Wang, L. Hua, A.Y. Chen, Y. Zhang, New method of lung cancer detection by saliva test using surface-enhanced Raman spectroscopy, Thorac. Cancer 9 (2018) 1556–1561, https://doi.org/10.1111/1759-7714.12837.
[45] S.Y. Feng, S.H. Huang, D. Lin, G.N. Chen, Y.J. Xu, Y.Z. Li, Z.F. Huang, J.J. Pan, R. Chen, H.S. Zeng, Surface-enhanced Raman spectroscopy of saliva proteins for the noninvasive differentiation of benign and malignant breast tumors, Int. J. Nanomed. 10 (2015) 537–547, https://doi.org/10.2147/IJN.S71811.
[46] L.W. Ma, Z.J. Zhang, X.G. Li, Non-invasive disease diagnosis using surface-enhanced Raman spectroscopy of urine and saliva, Appl. Spectrosc. Rev. 55 (2020) 197–219, https://doi.org/10.1080/05704928.2018.1562938.
[47] V. Moisoiu, M. Badarinza, A. Stefancu, S.D. Iancu, O. Serban, N. Leopold, D. Fodor, Combining surface-enhanced Raman scattering (SERS) of saliva and two-dimensional shear wave elastography (2D-SWE) of the parotid glands in the diagnosis of Sjogren's syndrome, Spectroc. Acta Pt. A-Mol. BioMol. Spectr. 235 (2020) 118267, https://doi.org/10.1016/j.saa.2020.118267.
[48] D.Z. Chen, J.Z. Gao, D. He, J.S. He, Y. Li, M. Zhang, W.Y. Li, X. Chen, X.H. He, T. Fu, Plasmonic bridge sensor enabled by carbon nanotubes and Au-Ag nano-rambutan for multifunctional detection of biomechanics and bio/chemical molecules, ACS Appl. Mater. Interfaces 15 (2023) 8783–8793, https://doi.org/10.1021/acsami.2c22634.
[49] J. Shi, S. Kim, P. Li, F. Dong, C. Yang, B. Nam, C. Han, E. Eig, L.L. Shi, S. Niu, J. Yue, B. Tian, Active biointegrated living electronics for managing inflammation, Science 384 (2024) 1023–1030, https://doi.org/10.1126/science.adl1102.
[50] Y.X. Hou, L. Wang, R. Sun, Y.A. Zhang, M.X. Gu, Y.H. Zhu, Y.B. Tong, X.Y. Liu, Z. X. Wang, J. Xia, Y.G. Hu, L. Wei, C.L. Yang, M. Chen, Crack-across-pore enabled high-performance flexible pressure sensors for deep neural network enhanced sensing and human action recognition, ACS Nano 16 (2022) 8358–8369, https://doi.org/10.1021/acsnano.2c02609.
[51] P. Li, Y.W. Wang, X.X. He, Y.Y. Cui, J.Y. Ouyang, J. Ouyang, Z.C. He, J.Y. Hu, X. J. Liu, H. Wei, Y. Wang, X.L. Lu, Q. Ji, X.Y. Cai, L. Liu, C. Hou, N. Zhou, S.W. Pan, X.R. Wang, H.M. Zhou, C.W. Qiu, Y.Q. Lu, G.M. Tao, Wearable and interactive multicolored photochromic fiber display, Light Sci. Appl. 13 (2024) 48, https://doi.org/10.1038/s41377-024-01383-8.
[52] Q.F. Shi, T.Y.Y. He, C. Lee, More than energy harvesting-combining triboelectric nanogenerator and flexible electronics technology for enabling novel micro-/nano-systems, Nano Energy 57 (2019) 851–871, https://doi.org/10.1016/j.nanoen.2019.01.002.
[53] X. Liu, J. Ma, X.M. Wu, L.W. Lin, X.H. Wang, Polymeric nanofibers with ultrahigh piezoelectricity via self -orientation of nanocrystals, ACS Nano 11 (2017) 1901–1910, https://doi.org/10.1021/acsnano.6b07961.
[54] H.M. Wang, Y. Zhang, X.P. Liang, Y.Y. Zhang, Smart fibers and textiles for personal health management, ACS Nano 15 (2021) 12497–12508, https://doi.org/10.1021/acsnano.1c06230.
[55] X.Y. Jiang, C. Shi, Z. Wang, L.Z. Huang, L.F. Chi, Healthcare monitoring sensors based on organic transistors: surface/interface strategy and performance, Adv. Mater. 36 (2023) 2308952, https://doi.org/10.1002/adma.202308952.
[56] M. Chen, J. Liu, P. Li, H. Gharavi, Y.X. Hao, J.Y. Ouyang, J.Y. Hu, L. Hu, C. Hou, I. Humar, L. Wei, G.Z. Yang, G.M. Tao, Fabric computing: concepts, opportunities, and challenges, Innovation 3 (2022) 100340, https://doi.org/10.1016/j.xinn.2022.100340.
[57] T. Sun, C. Yao, Z. Liu, S. Huang, X. Huang, S. Zheng, J. Liu, P. Shi, T. Zhang, H. Chen, H.-j Chen, X. Xie, Machine learning-coupled vertical graphene triboelectric pressure sensors array as artificial tactile receptor for finger action recognition, Nano Energy 123 (2024) 109395, https://doi.org/10.1016/j.nanoen.2024.109395.



Dongzhen Chen earned his M.S. and Ph.D. from Xi'an Jiaotong University in 2014 and 2018, respectively. Since 2018, he joined the faculty at Xi'an Polytechnic University. He is now an associate professor of School of Materials Science & Engineering, Xi'an Polytechnic University. His current research is focused on the surface functionalization of fibers, wearable sensing and health detection.



Yang Li earned his Master's degree in Materials Science and Engineering from Xi'an Polytechnic University in 2023. He is now a research and development engineer at Xiamen bolion Technology Co., Ltd. His main research areas are wearable sensors and flexible circuit boards.



Jianzhao Gao received his B.S. in Electrical Engineering and Automation from Northeast Electric Power University in 2017 and is currently pursuing his M.S. at Xi'an Polytechnic University. His research interests include developing wearable sensors and program algorithms for biometric recognition.



Meng Zhang entered medical school of Xi'an Jiaotong University in 2007. She received the B.S., M.S. and Ph.D. from Xi'an Jiaotong University in 2012, 2014 and 2018, respectively. She is attending doctor in department of Neurology in the 1st Affiliated Hospital of Xi'an Jiaotong University. She visited University of California, San Francisco in 2014–2015. Her research interests lie in neurodegenerative diseases and movement disorders.



Junhao Liang obtained his Ph.D. from Northwestern Polytechnical University in 2018. Since then, he has joined the faculty at Xi'an Polytechnic University and is currently an associate professor at the School of Materials Science and Engineering. His current research focuses on the fields of flexible wearables, three-dimensional textile composites preform weaving technology, and the formation methods of new modern textile composites.



Tao Fu received the Ph.D. degree in Materials Science and Engineering from Xi'an Jiaotong University in 2003. He is now an associate professor in School of Life Science and Technology of the same university. He had visited The University of Adelaide, Australia in 2014–2015. His research interests lie in biomaterials, biocoatings, biosensors, fluorescent probes, and thin films.



Xiaoming Wu is an associate professor at the School of Life Science and Technology at Xi'an Jiaotong University since 2015. With a Ph.D. in biomedical engineering, he has dedicated his career to the intersection of biomedical engineering and bioinformatics. He is a principal investigator on multiple research grants focused on the application of bioinformatics to genome sequence analysis, gene expression analysis and personalized medicine.



Xinhai He earned his Ph.D. from Northwestern Polytechnical University in 2012. He is now a professor of School of Materials Science & Engineering, Xi'an Polytechnic University. He obtained the honor of "famous teacher" in Shaanxi Province. He holds the director of Xi'an Key Laboratory of "Xi'an Key Laboratory of Textile Composites". His current research is focused on composite materials weaving and functionalization.



Liangjun Xia received his master degree from Wuhan Textile University under the supervision of Prof. Weilin Xu, and obtained Ph.D, degree from Deakin University, Australia. He is a distinguished professor at the State Key Laboratory of New Textile Materials and Advanced Processing Technologies, Wuhan Textile University, China. His current research interests mainly include the design of functional fiber-based materials for power sources and smart textiles.



Weilin Xu is an Academician of the Chinese Academy of Engineering. Prof. Xu is currently serving as the director of the State Key Laboratory of New Textile Materials and Advanced Processing Technologies at Wuhan Textile University, China. His research interests include advanced functional materials advanced spinning technologies, biomedical materials, and smart textiles.